

A Tight Connection Between Direct and Indirect Detection of Dark Matter through Higgs Portal Couplings to a Hidden Sector

Chiara Arina,^{*} François-Xavier Josse-Michaux,[†] and Narendra Sahu[‡]

Service de Physique Théorique, Université Libre de Bruxelles, 1050 Brussels, Belgium

We present a hidden abelian extension of the Standard Model including a complex scalar as a dark matter candidate and a light scalar acting as a long range force carrier between dark matter particles. The Sommerfeld enhanced annihilation cross-section of the dark matter explains the observed cosmic ray excesses. The light scalar field also gives rise to potentially large cross-sections of dark matter on the nucleon, therefore providing an interesting way to probe this model simultaneously at direct and indirect dark matter search experiments. We constrain the parameter space of the model by taking into account CDMS-II exclusion limit as well as PAMELA and FermiLAT data.

I. INTRODUCTION

The existence of dark matter (DM) in the present Universe has been firmly supported by a range of evidences [1]. The prime among them are galaxy rotation curves, large scale structure, cosmic microwave background and gravitational lensing. However, the identity of DM within the Standard Model (SM) of particle physics is still missing. Therefore, its experimental verification is expected to be a new discovery and a strong indication for physics beyond the SM.

Recently the Cryogenic DM Search (CDMS) Collaboration [2] in the Soudan mine reported the observation of two events compatible with a positive dark matter detection at 1.64σ confidence level (C.L.). The DAMA/LIBRA [3] experiment claims an evidence of DM in its modulated signal at 8.8σ C.L. Several other direct detection experiments are running and setting upper bounds, including EDELWEISS-II [4], ZEPLIN-II [5], XENON-10 [6] and Cresst-III [7]. The Xenon collaboration will soon release the data from the first run of the Xenon100 experiment [8] and superCDMS is planned.

A significant amount of effort has also been devoted to detection of DM through indirect searches. For example, the PAMELA collaboration [9] reported an unexpected rise of the positron fraction compared to that of the galactic background at energies above 10 GeV, while confirming the earlier results of AMS [10] and HEAT [11]. Similarly the HESS [12] and Fermi Large Area Telescope (FermiLAT) [13] collaborations also reported an excess of electron plus positron flux with respect to the galactic background at energies above 100 GeV, but without confirming the spectral features observed by the balloon-based experiments ATIC [14] and PPB-BETS [15]. It has been widely interpreted that DM could be a viable candidate for the observed cosmic ray anomalies, although they could be explained by astrophysical sources [16].

In light of the above experimental results, several models have been considered in the literature, which leave signatures at either direct [17] or indirect [18, 19] DM searches. Typically, for a given model, the predictions for direct and indirect signatures of DM depend on different parts of the parameter-space, and the derived constraints thus do not overlap. However, in some models the same couplings are responsible for both the scattering of DM on the nucleon and large annihilation cross sections, in which case an interesting complementarity between direct and indirect searches exists [20, 21].

A simple possibility is to consider singlet extensions of the SM, in which the DM is a singlet scalar [22], coupled to the SM Higgs particle through the so-called Higgs portal [23], namely the Higgs to DM quartic coupling (see also doublet extensions of the SM [24]). Depending on the strength of this portal, the singlet can account for the observed relic density, $\Omega_{\text{DM}} h^2 \sim 0.1$ [25]. Furthermore, through the Higgs portal coupling, DM scatters with the nucleon and is thereby constrained by direct searches, as well as annihilates into SM fermions which can be observed at indirect detection experiments [20, 21].

The anomalous positron and electron fluxes observed by PAMELA and FermiLAT require a large enhancement of current DM annihilations. In their minimal versions [22], the singlet extensions cannot reproduce such features. Furthermore, in these models, the stability of DM is supported by an *ad hoc* discrete symmetry. In this paper, we study a model which naturally solves these issues. We introduce a hidden sector gauged under an Abelian $U(1)_H$ [26]-

^{*}Electronic address: carina@ulb.ac.be

[†]Electronic address: fxjossemichaux@gmail.com

[‡]Electronic address: Narendra.Sahu@ulb.ac.be

[27], containing two complex scalars Φ and S . While all SM fields are hidden sector singlet, the extra scalars are singlet under the SM but charged under $U(1)_H$. This model provides all the ingredients for a viable DM model with potentially large direct and indirect detection signals.

The paper is organized as follows. In Sec. II we present the model, with particular attention to the mass spectrum and mixings in the scalar sector. The model parameter space is then examined in Sec. III and constrained by requiring the relic density of the DM candidate to be in the WMAP7 range. Sections IV and V describe the phenomenology of the model in light of the present DM searches: CDMS-II, XENON10, PAMELA and FemiLAT. First, in Sec. IV, we discuss the direct detection bounds constraining the hidden sector parameter space and the interplay with the indirect detection. Then, in Sec. V, we investigate the indirect detection bounds, and give the results in terms of positron and electron excesses. The conclusions are presented in Sec. VI.

II. THE MODEL

Assuming a non-trivial charge assignment under the hidden Abelian $U(1)_H$ for the extra scalars S and Φ , $q_H(S) = 3$ and $q_H(\Phi) = 2$, the most general scalar potential is given by:

$$V(H, S, \Phi) = -\mu_H^2 H^\dagger H + \lambda_H (H^\dagger H)^2 + \mu_S^2 S^\dagger S + \lambda_S (S^\dagger S)^2 - \mu_\Phi^2 \Phi^\dagger \Phi + \lambda_\Phi (\Phi^\dagger \Phi)^2 + f_{HS} H^\dagger H S^\dagger S + f_{H\Phi} H^\dagger H \Phi^\dagger \Phi + f_{S\Phi} S^\dagger S \Phi^\dagger \Phi. \quad (1)$$

The hidden sector couples to the SM via Higgs portals, as schematically depicted in Fig.(1). We assume that all

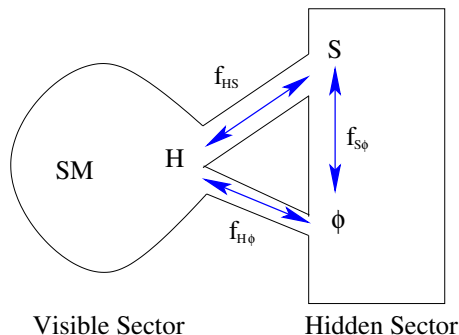


FIG. 1: Schematic representation of Higgs portal couplings to a hidden sector.

parameters are real and positive. The field Φ acquires a nonzero vacuum expectation value (vev), which triggers the breaking of $U(1)_H$ to a remnant Z_2 symmetry under which all fields are even but S . The latter does not develop any nonzero vev and hence can be a dark matter candidate, being stabilized by the Z_2 symmetry.

It is remarkable that almost all the parameters in this model are well constrained by both direct and indirect searches, as we will see in great details below. The relic density of S is obtained through its annihilations into H and Φ via f_{HS} and $f_{S\Phi}$, respectively. These two couplings also enter in the spin-independent cross section of DM on nucleon and hence are strongly constrained by direct DM searches. The field Φ gives rise to a long range attractive force between S particles, thus boosting the current S annihilations, while keeping the relic abundance unchanged. As a result $f_{S\Phi}$ gets strongly constrained from indirect DM searches. After Φ acquires a vev, it mixes with the SM Higgs through $f_{H\Phi}$. Φ is destabilized and consequently decays into SM fermions through the same coupling. While $f_{H\Phi}$ should not be too small for Φ to decay before the onset of big bang nucleosynthesis (BBN), a too large H - Φ mixing is excluded by constraints coming from LEP-II on the ratio of the invisible-to-visible Higgs decay [28].

A. Masses and Mixings of Hidden Sector Fields

From the scalar potential in Eq. (1), let us derive the quantities relevant for this study. First of all, vacuum stability requires, besides positive quartic couplings, that $4\lambda_H\lambda_S\lambda_\Phi + f_{HS}f_{H\Phi}f_{S\Phi} \geq \lambda_H f_{S\Phi} + \lambda_\Phi f_{HS} + \lambda_S f_{H\Phi}$. The electroweak symmetry breaking occurs when the SM Higgs acquires a vev $\langle H \rangle = v/\sqrt{2}$, while $U(1)_H$ is broken to a surviving Z_2 symmetry when Φ acquires a vev $\langle \Phi \rangle = u/\sqrt{2}$. In the unitary gauge, the quantum fluctuations around the minimum

are parametrized as

$$H = \frac{1}{\sqrt{2}} \begin{pmatrix} 0 \\ v + h \end{pmatrix} \quad \text{and} \quad \Phi = \frac{1}{\sqrt{2}}(u + \phi), \quad (2)$$

where h and ϕ are physical real scalars, the unphysical degrees of freedom being eaten by the longitudinal component of the SM gauge bosons and of the Z' associated with $U(1)_H$. Minimization of the scalar potential in Eq. (1) enforces

$$\frac{v}{\sqrt{2}} = \left(\frac{2\mu_H^2 \lambda_\phi - \mu_\phi^2 f_{H\phi}}{4\lambda_H \lambda_\phi - f_{H\phi}^2} \right)^{1/2}, \quad \frac{u}{\sqrt{2}} = \left(\frac{2\mu_\phi^2 \lambda_H - \mu_H^2 f_{H\phi}}{4\lambda_H \lambda_\phi - f_{H\phi}^2} \right)^{1/2}. \quad (3)$$

This minimum is the global one if $f_{H\phi}^2 \leq 4\lambda_H \lambda_\phi$. The two real scalars h and ϕ mix with each other and the mass matrix in the basis spanned by (h, ϕ) is given by:

$$\mathcal{M}^2 = \begin{pmatrix} 2\lambda_H v^2 & f_{H\phi} uv \\ f_{H\phi} uv & 2\lambda_\phi u^2 \end{pmatrix}. \quad (4)$$

Assuming $f_{H\phi} \ll 1$, the mixing angle between h and ϕ is suppressed:

$$\theta_m \sim -\frac{f_{H\phi} uv}{2(\lambda_H v^2 - \lambda_\phi u^2)} \ll 1. \quad (5)$$

In terms of (h, ϕ) , the mass eigenstates h_1 and h_2 read:

$$h_1 \sim h + \theta_m \phi \quad \text{and} \quad h_2 \sim \phi - \theta_m h. \quad (6)$$

Consequently h_1 is mostly the SM Higgs field, while h_2 is the light scalar. Their respective masses are:

$$M_{h_1}^2 \simeq 2\lambda_H v^2 \quad \text{and} \quad M_{h_2}^2 \simeq 2\lambda_\phi u^2 \left(1 - \frac{f_{H\phi}^2}{4\lambda_H \lambda_\phi} \right). \quad (7)$$

Because of the small mixing, the current experimental bounds [28, 29] on the SM Higgs mass apply on M_{h_1} . Hereafter, in all numerical evaluations we take $M_{h_1} = 120$ GeV. However, we note that our results are quite insensitive to the Higgs Mass. The light scalar field h_2 is the main product of S annihilations at the present epoch. In order to avoid overproduction of high-energy gamma rays from the decay of h_2 , $M_{h_2} < 2m_\pi$ is required: we take $M_{h_2} = 240$ MeV as numerical reference value. We then have $\lambda_H v^2 \gg \lambda_\phi u^2$.

The DM mass is given by:

$$M_S^2 = \mu_S^2 + \frac{f_{S\phi}}{2} u^2 + \frac{f_{HS}}{2} v^2, \quad (8)$$

which is varied from 10 GeV to 1 TeV in the following.

The hidden sector is gauged under the Abelian $U(1)_H$ and contains an extra gauge boson Z' . Although SM particles are singlet under $U(1)_H$, through the kinetic mixing of Z' with the hypercharge gauge boson, they can couple to Z' . The relevant part of the Lagrangian then reads:

$$\mathcal{L}_{Z'} = -\frac{1}{4} F_{\mu\nu}^H F^{H\mu\nu} - \frac{\chi}{2} F_{\mu\nu}^Y F^{H\mu\nu} + |(\partial_\mu - 2ig_H Z'_\mu)\Phi|^2 + |(\partial_\mu - 3ig_H Z'_\mu)S|^2, \quad (9)$$

where g_H is the hidden sector coupling constant, $F_{\mu\nu}^Y$ and $F_{\mu\nu}^H$ are the field strength tensors associated with $U(1)_Y$ and $U(1)_H$ respectively and χ parameterizes the kinetic mixing between the $U(1)$ symmetries.

For an invisible Z' , the kinetic mixing is expected to be $\chi \sim 10^{-4}$ - 10^{-2} at the electroweak scale. The mass of Z' is given by $M_{Z'} = 2g_H u$ and we take 600 GeV as a reference numerical value. The parameter u is then lower bounded by the requirement of perturbative $U(1)_H$ gauge coupling: $u \gtrsim 85$ GeV. For the chosen value of the Z' mass, the electroweak precision measurement constraints the kinetic mixing to be $\chi \leq 0.036$ [30]. Through Z - Z' mixing, the DM can scatter on nuclei. The corresponding cross section may exceed the current experimental bounds for $\chi \gtrsim 0.01$. When $M_{Z'} \lesssim M_S$ the dark gauge boson is produced in S annihilations. For large χ , this would lead to significant antiproton fluxes in the cosmic ray which is in contradiction with PAMELA data [31]. In the following we assume $\chi \sim 10^{-4}$ and so Z' effects are negligible.

Assuming $M_{Z'} = 600$ GeV with $g_H \sim \mathcal{O}(1)$ while $M_{h_2} = 240$ MeV implies a strong tuning of the model parameters, with $\mu_\phi = 120$ MeV $\ll u \sim 300$ GeV and $\lambda_\phi \sim 10^{-7}$. Reducing this tuning can be achieved by either increasing the hidden scalar boson mass, or by lowering $M_{Z'}$ as well as M_S . However, in those cases, predictions of the model turn out to be very different from those we discuss hereafter. By increasing M_{h_2} we possibly face an antiproton overproduction in DM current annihilations, in which case the corresponding cross section should be suppressed compared to PAMELA requirements. In this case, still, the model can afford a viable DM candidate but lacks predictivity. Another way to reduce the tuning is to lower $M_{Z'}$ or M_S . With a lighter DM, the PAMELA cosmic ray spectrum cannot be accounted for, while with a lighter Z' the model is in conflict with direct detection experiments. Therefore, in the following, we assume a certain amount of tuning, allowing the model to be predictive and probed by both direct and indirect detection experiments.

B. Astrophysical and collider constraints

We now discuss some relevant constraints on the hidden sector coming from astrophysics and the electroweak precision measurements. The scalar field h_2 decays to SM fermions through Φ - H mixing; its decay rate is approximately given by:

$$\Gamma_{h_2} \simeq \sum_{2m_f < M_{h_2}} \frac{M_{h_2} \theta_m^2}{8\pi} \frac{2m_f^2}{v^2}. \quad (10)$$

The lifetime of h_2 is then estimated as

$$\tau_{h_2} \simeq 0.1s \times \frac{2m_\pi}{M_{h_2}} \times \left(\frac{\theta_m}{10^{-7}} \right)^{-2}. \quad (11)$$

Thus, demanding that h_2 decays before the onset of BBN $\tau_{h_2} \lesssim \tau_{BBN} \sim 0.1s$ [32], θ_m should be bigger than 10^{-7} . Equivalently a lower bound on the Higgs portal coupling $f_{H\phi}$ is inferred:

$$f_{H\phi} \gtrsim 10^{-8} \times \left(\frac{M_{h_1}}{120 \text{ GeV}} \right)^2 \left(\frac{u}{600 \text{ GeV}} \right)^{-1}. \quad (12)$$

Assuming that h_2 dominantly decays to $\mu^+\mu^-$, a strong constraint on θ_m can be obtained from the B -meson decay. From the branching ratio $BR(B \rightarrow \mu^+\mu^-X) < 3.2 \times 10^{-4}$ [27],[33], one infers an upper bound on θ_m to be $|\theta_m| \lesssim 10^{-2}$ [34]. This in turn gives

$$f_{H\phi} \lesssim 10^{-3} \times \left(\frac{600 \text{ GeV}}{u} \right) \left(\frac{M_{h_1}}{120 \text{ GeV}} \right)^2. \quad (13)$$

Since h_2 is very light, the mixing angle never saturates the above bound. For the same reason, the electroweak precision measurements on the S, T and U parameters do not receive any significant contributions from h_2 [35].

III. ANNIHILATION CROSS-SECTION OF THE S DM AT FREEZE-OUT AND AT PRESENT EPOCH

A. Relic density

In the early universe the S particles maintain their thermal equilibrium through the scattering processes: $S^\dagger S \rightarrow h_2 h_2$ and $S^\dagger S \rightarrow$ SM particles. In Fig. (2), we display ratios of the dominant annihilation channels with respect to the total annihilation cross-section σ_{tot} , as a function of the DM mass. In case of $f_{HS} \gg f_{S\phi}$ (left panel) the dominant channel is $S^\dagger S \rightarrow \bar{f}f$ (blue dashed curve) until the W^+W^- (black dot-long dashed solid) and ZZ (black dot-dashed) thresholds are reached. These two processes dominate the behavior of S annihilations up to 120 GeV, when $S^\dagger S \rightarrow h_1 h_1$ (green dashed curves) takes the upper hand. The situation is reversed as soon as $f_{S\phi} \gtrsim f_{HS}$ (central and right panels). The annihilation into $h_1 h_1$ is competitive only for equal Higgs portal couplings, while for $f_{S\phi} = 10f_{HS}$, $S^\dagger S \rightarrow h_2 h_2$ (red solid curves) dominates in all the DM mass range, apart from the Higgs pole.

As the universe expands, the temperature of the thermal bath gradually falls; at $T_D \simeq M_S/25$, S gets decoupled and starts redshifting. The relic abundance of DM can be evaluated by solving the Boltzmann equation for the S number density:

$$\frac{dn_S}{dt} + 3n_S H(t) = -\langle \sigma |v_{\text{rel}}| \rangle (n_S^2 - n_S^{\text{eq}2}), \quad (14)$$

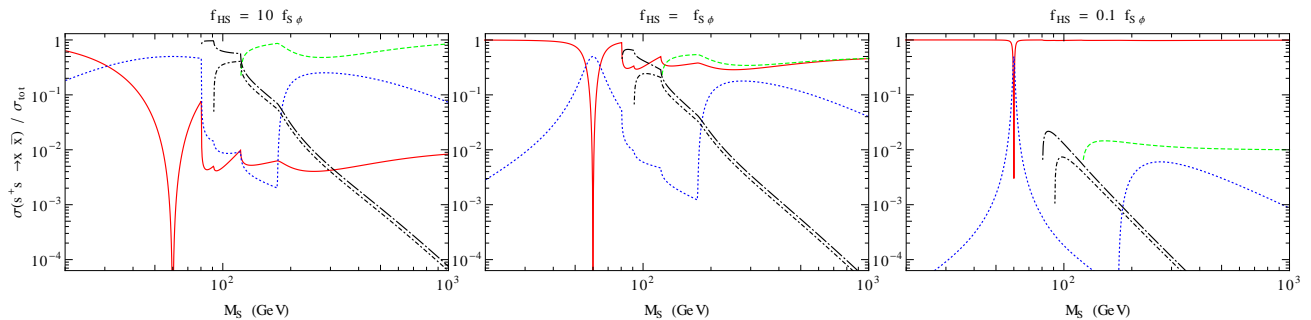


FIG. 2: Ratios of the leading annihilation channels of S on the total annihilation cross-section are shown as a function of M_S : in red solid ($S^\dagger S \rightarrow h_2 h_2$), in green dashed ($S^\dagger S \rightarrow h_1 h_1$), in blue dotted ($S^\dagger S \rightarrow f \bar{f}$), in black dot-dashed ($S^\dagger S \rightarrow W^+ W^-$) and in black dot-long dashed ($S^\dagger S \rightarrow ZZ$).

where $H(t)$ is the Hubble expansion parameter and $\langle \sigma |v_{\text{rel}}| \rangle$ is the thermal average of the total annihilation cross-section.

To accurately evaluate the DM relic density, we solve Eq.(14) by using micrOMEGAs [36]. The model has been implemented in micrOMEGAs through FeynRules [37]. The parameter space is chosen as follows. The physical Higgs masses are fixed at $M_{h_1} = 120$ GeV and $M_{h_2} = 240$ MeV, while the other relevant parameters are varying randomly within their allowed ranges: u from 10 GeV to 1 TeV and μ_s from 1 GeV to 500 GeV. The portal couplings $f_{S\phi}$ and f_{HS} vary from 10^{-3} to $\sqrt{4\pi}$, the perturbative upper bound, while $f_{H\phi}$ varies from 10^{-7} to 10^{-4} . We also constrain the lifetime of h_2 to be less than 0.1s.

Demanding that the relic abundance of DM should satisfy the WMAP7 constraints [25] at 3σ C.L., given by

$$\Omega_{\text{DM}} h^2 = 0.0941 - 0.1277, \quad (15)$$

we show in Fig. (3) the resulting scatter plots in the plane of $f_{S\phi}$ and f_{HS} against M_S .

The requirement of having the correct relic density fixes the balance between the two Higgs portal couplings $f_{S\phi}$ and f_{HS} and hence between the different annihilation channels. In the left panel of Fig. (3), as long as $M_S \lesssim M_{h_1}/2$, we clearly see that the $S^\dagger S \rightarrow h_2 h_2$ channel dominates. Near the Higgs resonance, $M_S \sim M_{h_1}/2$, lower values of the portal couplings are allowed, but at the pole, annihilations are too efficient and the relic density gets suppressed. For $M_{h_1}/2 \lesssim M_S \lesssim M_W$, the DM dominantly annihilates into light SM fermions, mostly $b\bar{b}$ pairs. For $M_W \lesssim M_S \lesssim M_{h_1}$, the $S^\dagger S \rightarrow W^+ W^-$ and $S^\dagger S \rightarrow ZZ$ channels, mediated by h_1 , strongly constrain f_{HS} , as can be seen in Fig. (3) (right panel). For larger DM masses, the annihilation channels $S^\dagger S \rightarrow h_1 h_1$ and $S^\dagger S \rightarrow t\bar{t}$ are also allowed. For such large DM masses, f_{HS} is more constrained than $f_{S\phi}$. The latter can indeed take values up to the perturbative bound, while the former is upper bounded at 1.

Resuming, on the whole range of DM mass, $f_{S\phi}$ typically takes values of the same order or larger than f_{HS} . This corresponds to middle and right plots of Fig.(2), and implies that the DM is preferably annihilating into h_2 , as can be inferred from the approximate cross-sections:

$$\begin{aligned} \langle \sigma |v_{\text{rel}}| \rangle (S^\dagger S \rightarrow h_2 h_2) &\simeq \frac{f_{S\phi}^2}{64\pi M_S^2}, \\ \langle \sigma |v_{\text{rel}}| \rangle (S^\dagger S \rightarrow h_1 h_1) &\simeq \frac{1}{64\pi} \frac{f_{HS}^2}{M_S^2} \left(1 - \frac{M_{h_1}^2}{M_S^2} \right)^{1/2}. \end{aligned} \quad (16)$$

Thus we see that both portal couplings f_{HS} and $f_{S\phi}$ are constrained from the requirement of obtaining the right DM relic density. Interestingly, these couplings also enter in the t-channel Higgs-mediated scattering $Sf \rightarrow Sf$, which is relevant for the direct detection of DM, as we discuss in the next section.

B. Sommerfeld enhancement

The observed relic density of DM can be obtained for an annihilation cross-section $\langle \sigma |v_{\text{rel}}| \rangle_D \simeq 3 \times 10^{-26} \text{cm}^3 \text{s}^{-1}$ at the decoupling epoch, $T_D \sim M_S/25$. However, at the present epoch, such a cross-section is too small to explain the anomalous cosmic ray fluxes observed by PAMELA and FermiLAT. Several mechanisms have been invoked in

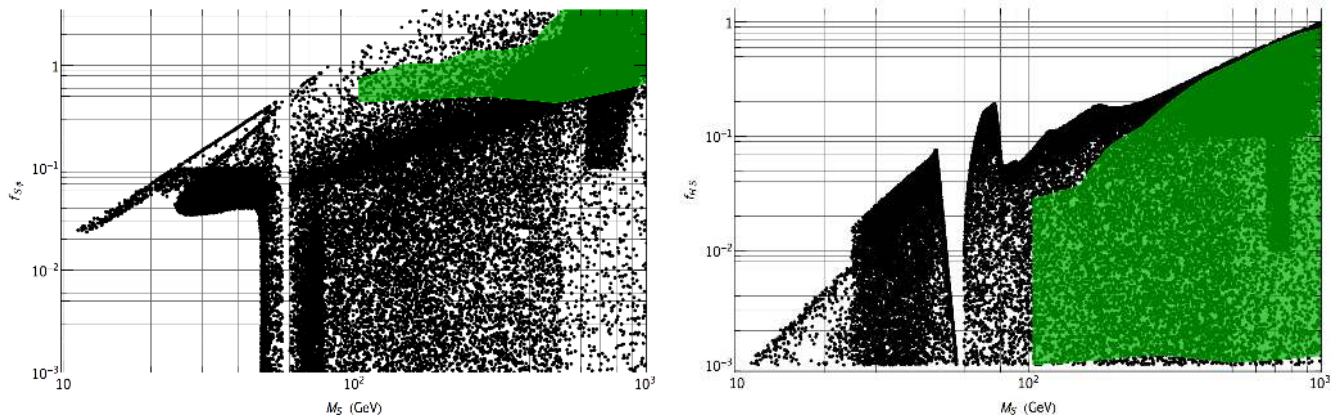


FIG. 3: Scatter plot for the relic abundance of S . In the left (right) panel the solutions that satisfy $\Omega_{\text{DM}} h^2 = 0.0941 - 0.1277$ are shown as black points in the plane M_S versus $f_{S\phi}$ (f_{HS}). The green (gray) region denotes points with boost factors compatible with indirect DM searches.

the literature to boost it. A natural enhancement may occur due to the local overdensities of DM in clumps [38], but estimates show that the resulting boost of the annihilation cross-section is too small to account for the observed cosmic ray fluxes. Two different mechanisms, arising from particle physics, also exist: either a Breit-Wigner resonance of the annihilation cross-section [27],[39], or the Sommerfeld effect [40]. In this model, the latter naturally occurs because of the presence of h_2 . The light scalar h_2 acts as a long range attractive force carrier between the DM particles. If S kinetic energy is small enough, the attractive interaction becomes relevant and induces an enhancement of the annihilation cross section. Defining the reduced DM bound-state wave-function as ψ , the corresponding boost is computed by solving the radial Schrödinger equation:

$$\psi(r)'' - M_S V(r)\psi(r) + M_S^2 \beta^2 \psi(r) = 0, \quad (17)$$

where $\beta = v_{\text{rel}}/c$ is the DM relative velocity, and $V(r)$ is the attractive Yukawa potential:

$$V(r) = -\frac{\alpha}{r} e^{-M_{h_2} r}, \quad \text{with} \quad \alpha = \left(\frac{f_{S\phi} u}{M_S} \right)^2 \frac{1}{8\pi}. \quad (18)$$

We solve Eq.(17) using the boundary condition $\psi'(\infty) = iM_S \beta \psi(\infty)$. The Sommerfeld boost is then given by

$$S_e = \left| \frac{\psi(\infty)}{\psi(0)} \right|^2. \quad (19)$$

To consider the enhancement at present time, one should integrate over the velocity distribution of DM in the Earth's neighborhood:

$$\langle S_e \rangle = \mathcal{N}_{\text{norm}} \int_0^{v_{\text{esc}}} dv_{\text{rel}} \frac{v_{\text{rel}}^2}{v_0^3} e^{-v_{\text{rel}}^2/v_0^2} S_e(v_{\text{rel}}, \alpha, M_{h_2}/M_S), \quad (20)$$

with mean velocity $v_0 = 220$ km/s, escape velocity $v_{\text{esc}} = 650$ km/s and a normalization factor $\mathcal{N}_{\text{norm}}$ for a smooth maxwellian halo. The boost factor is then only a function of $u \times f_{S\phi}$, M_S and M_{h_2} . Therefore, for a given DM mass, $\langle S_e \rangle$ is degenerate with respect to $f_{S\phi}$ and u , the hidden sector breaking scale. The effective DM annihilation cross-section then reads

$$\langle \sigma |v_{\text{rel}}| \rangle = \langle S_e \rangle \times \langle \sigma |v_{\text{rel}}| \rangle_D. \quad (21)$$

In Fig. (3) the region of the parameters giving rise to boost factors from 20 up to ~ 2000 is displayed by a green (gray) region. This is the range of enhancement required to explain the observed cosmic ray anomalies for a DM of mass (100 - 1000) GeV, compatible with current cosmological and astrophysical constraints, as discussed in Sec. V. On the left panel we see that only large values for $f_{S\phi}$ are allowed, ranging from 10^{-1} up to $2\sqrt{\pi}$. This is expected by the behavior of the Sommerfeld enhancement $\propto \alpha/\beta$. As mentioned before, the requirement of having a good relic density fixes the balance between the two portal couplings. In the right panel of Fig.(3), the values of f_{HS} in the green (gray) region correspond to the values of $f_{S\phi}$ giving rise to a correct boost factor, although the Sommerfeld effect does not depend on f_{HS} . For 100 GeV $\lesssim M_S \lesssim 200$ GeV, the largest values of f_{HS} are not allowed because they dominate S annihilations, which in turn corresponds to lower values of $f_{S\phi}$.

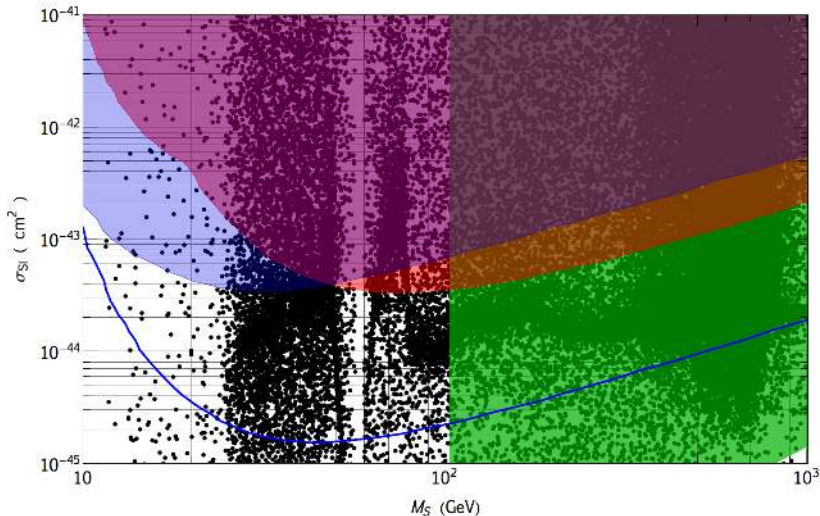


FIG. 4: Scatter plot for the direct detection of S particles in the plane M_S versus σ_{SI} . Solutions with a relic density in the WMAP7 range are depicted by black points; the red region (dark grey) is excluded at 90% C.L. by CDMS-II, while the blue region (light gray) is excluded at 90% C.L. by XENON10. The solid blue curve is the forecast upper bound for the Xenon100 experiment. The green region (gray) denotes points that in addition provide a correct boost factor.

IV. CDMS-II EVENTS AND S DARK MATTER

A. Experimental upper bounds

The CDMS collaboration has recently published the analysis of the final run of the CDMS-II experiment [2]. After the background subtraction and cuts, two events survive, respectively at 12.3 keV and 15.5 keV recoil energies. The significance of the two events being a DM signal is at 1.64σ C.L., namely there is 23% probability that these are of more common origin, such as cosmogenic or neutron background. In Ref. [41], it has been shown that if the two events are taken to be DM signal, the 1.64σ region will prefer light dark matter candidates, with an upper bound on the mass around 60-80 GeV. If we consider the 90% C.L. region to constraint the DM mass, then only an upper bound can be set. We approach the analysis of the two events of the CDMS-II in a conservative way, finding a 90% C.L. exclusion limit with the maximum gap method [42].

In addition the upper bound from the XENON10 experiment [6] is taken into account, which is the most constraining one together with CDMS-II, in the case of spin-independent elastic interaction on nucleon. Using the data of the 2007 run, reanalyzed as in Ref. [43], and the maximum gap method, we infer the 90% C.L. upper bound. We also consider the prediction for the first run of the XENON100 experiment, following Ref. [8].

B. The elastic spin-independent S cross-section

The interaction of S on the nucleon gives rise to a coherent spin-independent elastic scattering, mediated at tree level by the scalars of the model, the SM Higgs particle and h_2 . This cross section reads:

$$\sigma_{\text{SI}} = \frac{\mu_n^2}{\pi M_S^2} m_n^2 f_n^2 \left| \frac{1}{2} \frac{f_{HS}}{M_{h_1}^2} + \frac{1}{2} \frac{f_{S\phi} u \theta_m}{M_{h_2}^2 v} \right|^2, \quad (22)$$

where m_n is the nucleon mass and μ_n is the nucleon-DM reduced mass. The parameter f_n indicates the effective Higgs nucleon interaction, $f_n m_n = \langle n | \sum_q m_q \bar{q}q | n \rangle$, where the sum runs over all the quark flavor. The f_n factor introduces hadronic uncertainties in the elastic cross section: its value vary within a wide range $0.14 < f_n < 0.66$, as quoted in Refs. [44]. Hereafter we take f_n to be $1/3$, the central value.

From the Lagrangian in Eq. (9), the S particle couples directly to the hidden gauge boson and through the kinetic mixing it communicates to the SM fermions. This results in an additional DM-nucleon scattering. Neglecting terms

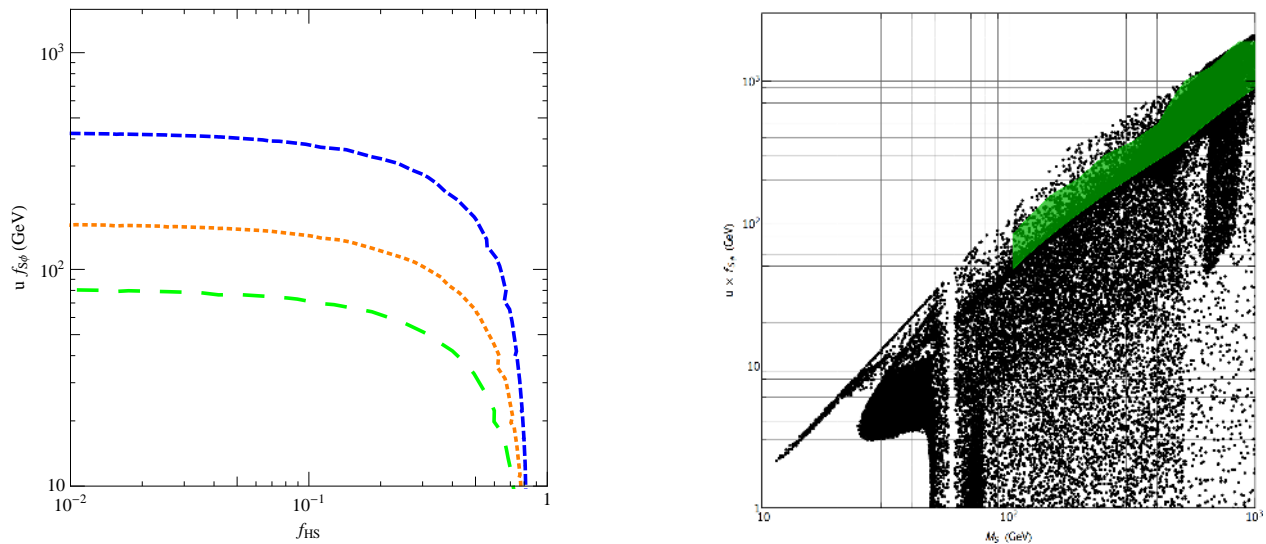


FIG. 5: Left panel: maximal σ_{SI} value in the plane f_{HS} and $u \times f_{S\phi}$ for $M_S = 400$ GeV, $\theta_m = 1.9 \times 10^{-6}$ (blue dashed curve), $\theta_m = 5 \times 10^{-6}$ (dotted orange line) and $\theta_m = 10^{-5}$ (green long dashed line). The region plane on the right-hand side of each curve is excluded by CDMS-II at 90% C.L.. Right panel: scatter plot in the plane of $u \times f_{S\phi}$ vs M_S . Black points give the required relic density, while the points in the green (gray) region give rise to a boost factor compatible with PAMELA anomaly.

of order χ^3 , the corresponding spin-independent cross section is approximately:

$$\sigma_n^{\text{SI}}(S_n \rightarrow Z' \rightarrow S_n) \simeq \frac{\mu_n^2}{A^2} \frac{g^2}{64\pi \cos^2 \theta_W} \frac{9}{M_{Z'}^2 u^2} \chi^2 \sin^2 \theta_W (A + 2Z)^2, \quad (23)$$

where A and Z are the mass and the atomic number of the nucleus and g is the $SU(2)_L$ coupling. The cross section is slightly dependent on the DM mass, through the reduced mass μ_n . For $M_{Z'} = 600$ GeV, the values of u we scanned over and for a maximal kinetic mixing $\chi = 0.036$, the cross-section value ranges from 10^{-45}cm^2 up to 10^{-43}cm^2 . As stated above, we fixed $\chi = 10^{-4}$, and consequently the cross section varies from 10^{-50}cm^2 up to 10^{-48}cm^2 , and is therefore a negligible correction to h_1 and h_2 contributions. It is then possible to constrain Higgs portal couplings thanks to direct detection searches.

The behavior of σ_{SI} as a function of the Higgs portal couplings is rather involved. Owing to the large mass differences between the two scalars, *cf.* Eq. (5), the mixing angle between h_2 and h_1 is small, of the order of $\theta_m \sim \mathcal{O}(10^{-6}-10^{-5})$. Even though $\theta_m \ll 1$, the second term in Eq. (22) is not negligible in the whole S mass range. With respect to the standard Higgs exchange, the h_2 contribution is enhanced due to its small mass, which compensates the smallness of its coupling to the nucleon. Note that this result is valid in general in models where a scalar with mass lighter than 1 GeV, typically the light force carrier of the Sommerfeld enhancement mechanism, mixes with the SM Higgs [20, 21].

The predictions for σ_{SI} are shown in Fig. (4) as a function of M_S , with all the points having a relic abundance in the WMAP7 range. The cross-section is enhanced respect to the standard Higgs exchange: a large region (red region) of the parameter space is not allowed by CDMS-II experiment. In the low mass range a portion of the parameter space is incompatible with the XENON10 upper bound, denoted by the blue (light gray) band. The green (gray) region describes the parameter space that leads to a large sommerfeld effect and boosts $\langle \sigma |v_{\text{rel}}| \rangle_D$. As described in the previous section, a large Sommerfeld enhancement calls for large $f_{S\phi}$ coupling. We can therefore constraint the parameter space yielding such a large boost factor with the direct detection bounds. As shown in Fig. (4), a large portion of the green (gray) region is excluded, but nonetheless a large portion is found compatible with direct detection constraints. We also show the prediction for the upcoming XENON100 first run (blue line): while it can probe a bigger portion of the hidden sector parameter space compatible with indirect detection, a large part can give DM to nucleon cross-section below the expected sensitivity.

On the left of Fig. (5), we show an illustrative example of the balance between the two contributions in Eq. (22), for a fixed DM mass $M_S = 400$ GeV. The maximum value of the elastic cross section compatible with CDMS-II is plotted, as a function of f_{HS} and $u \times f_{S\phi}$. In this plot, three different values of the mixing angle are depicted, $\theta_m = 1.9 \times 10^{-6}$ (blue dashed line), 5×10^{-6} (orange dotted line), and 10^{-5} (green long dashed line). First of all, for $f_{HS} \sim 1$, the SM Higgs exchange dominates and σ_{SI} is rather insensitive to θ_m . As f_{HS} decreases towards smaller values, the h_2 contribution becomes the leading one. For $f_{HS} \ll 1$, from Eq. (22) we see that σ_{SI} only depends on

the product $\theta_m \times u \times f_{S\phi}$. For $f_{HS} \sim 10^{-2}$, we then have that different values of the mixing angle imply different maximum values of $u \times f_{S\phi}$. Notice that, from Eqs. (18) and (20), the Sommerfeld enhancement is sensitive to the same combination $u \times f_{S\phi}$. The right panel of Fig. (5) shows the points giving the right relic abundance in the plane $u \times f_{S\phi}$ vs M_S , where again a green (gray) region highlights the values of interest for the indirect detection. For $f_{HS} = 10^{-2}$, a small mixing angle $\theta_m = 1.9 \times 10^{-6}$ allows for $u \times f_{S\phi} \simeq 410$ GeV, which is compatible with indirect detection constraints. Indeed, we see that for $M_S = 400$ GeV, $u \times f_{S\phi}$ should be in the 300 – 500 GeV range. Increasing θ_m calls for smaller values of $u \times f_{S\phi}$, and consequently lower $\langle S_e \rangle$ can be obtained. For $\theta_m = 5 \times 10^{-6}$, we see that $u \times f_{S\phi} \lesssim 160$ GeV, a value for which the boost factor is too small to account for the whole cosmic ray excesses. The situation is even worst for $\theta_m = 10^{-5}$ for which $u \times f_{S\phi} \lesssim 80$ GeV.

V. ELECTRON, POSITRON AND ANTIPROTON FLUXES FROM $S^\dagger S$ ANNIHILATION

As described in Sec. III, the annihilation of $S^\dagger S \rightarrow h_2 h_2$ and $S^\dagger S \rightarrow h_1 h_1$ will generate both positrons and antiprotons in the present Universe and could have been detected by various experiments such as PAMELA, HESS and FermiLAT. In the case S annihilates into h_2 , the final products are dominantly muons and antimuons resulting from the decay of h_2 , while in the latter case the final products are mostly hadrons. From Eq.(16), the ratio of S annihilation cross sections into h_1 to h_2 is

$$\frac{\langle \sigma |v_{\text{rel}}| \rangle (S^\dagger S \rightarrow h_1 h_1)}{\langle \sigma |v_{\text{rel}}| \rangle (S^\dagger S \rightarrow h_2 h_2)} \approx \left(\frac{f_{HS}}{f_{S\phi}} \right)^2. \quad (24)$$

As we see from Fig.(3), we typically have $f_{S\phi} \gtrsim 10 f_{HS}$ when we require that the annihilation cross-section is enhanced by a non-negligible boost factor. This is sufficient to suppress the antiproton flux over the positron one. Therefore, in what follows we will focus on the production and propagation of positrons in the Galactic medium.

A. Production and propagation of positrons

From S annihilations, h_2 is produced which then decays to muon and antimuon. They ultimately decay to electrons, positrons and neutrinos. As a result, equal numbers of electrons and positrons are produced from the annihilation of S particles. However, the background flux of electrons in the Galactic medium is significantly larger than the positron one. Therefore, it is easier to find signature of DM, if any, in the Galactic positron flux.

Once the positrons are produced in the Galactic halo where the DM concentration is large, they travel under the influence of the Galactic magnetic field which is assumed to be of the order of a few microgauss. The motion of positrons can then be thought of as a random walk. In the vicinity of the Solar System, the positron flux can be obtained by solving the diffusion equation [45]

$$\frac{\partial}{\partial t} f_{e^+}(E, \vec{r}, t) = Q(E, \vec{r}) + K_{e^+}(E) \nabla^2 f_{e^+}(E, \vec{r}, t) + \frac{\partial}{\partial t} [b(E) f_{e^+}(E, \vec{r}, t)], \quad (25)$$

where $f_{e^+}(E, \vec{r})$ is the number density of positrons per unit energy, E is the energy of positron, $K_{e^+}(E)$ is the diffusion constant, $b(E)$ is the energy-loss rate and $Q(E, \vec{r})$ is the positron source term. The latter, due to S annihilations, is given by:

$$Q(E, \vec{r}) = n_S^2(\vec{r}) \langle \sigma |v_{\text{rel}}| \rangle \frac{dN_{e^+}}{dE}. \quad (26)$$

In the above equation the fragmentation function dN_{e^+}/dE represents the number of positrons with energy E which are produced from the annihilation of S particles. We assume that the positrons are in steady state, i.e. $\partial f_{e^+}/\partial t = 0$. Then from Eq. (25), the positron flux in the vicinity of the solar system can be obtained in a semi-analytical form [45–47]

$$\Phi_{e^+}(E, \vec{r}_\odot) = \frac{v_{e^+}}{4\pi b(E)} (n_S)_\odot^2 \langle \sigma |v_{\text{rel}}| \rangle \int_E^{M_S} dE' \frac{dN_{e^+}}{dE'} I(\lambda_D(E, E')), \quad (27)$$

where $\lambda_D(E, E')$ is the diffusion length from energy E' to energy E and $I(\lambda_D(E, E'))$ is the halo function which is independent of particle physics. An analogous solution for the electron flux can also be obtained.

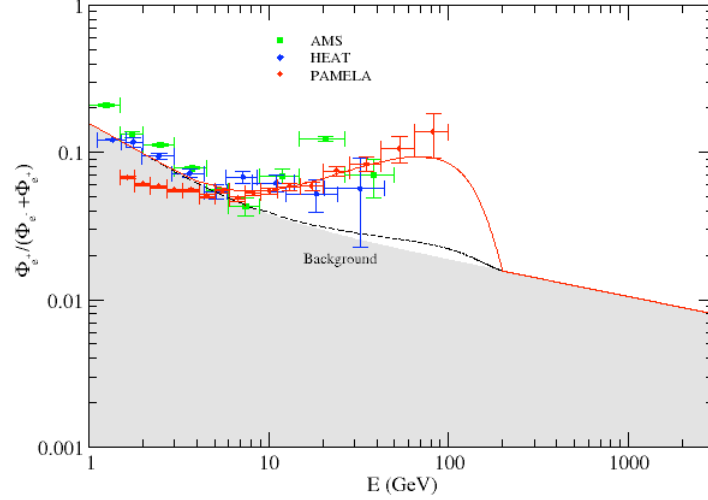


FIG. 6: Positron fraction from $S^\dagger S \rightarrow 2\mu^+\mu^-$ at $M_S = 400$ GeV. The red solid line (black dashed line) stands for the illustrative point 1 (2) quoted in Table I.

B. Background fluxes of electron and positron

Positrons in our galaxy are not only produced by S particle annihilations but also by the scattering of cosmic-ray protons with the interstellar medium [48]. The positrons produced from the later sources thus act as background for the positrons produced from DM annihilations. The background positron fraction can be defined as

$$\left(\frac{\Phi_{e^+}}{\Phi_{e^+} + \Phi_{e^-}} \right)_{\text{bkg}} = \frac{\Phi_{\text{sec}, e^+}^{\text{bkg}}}{\Phi_{\text{prim}, e^-}^{\text{bkg}} + \Phi_{\text{sec}, e^-}^{\text{bkg}} + \Phi_{\text{sec}, e^+}^{\text{bkg}}}, \quad (28)$$

where the primary and secondary electron fluxes, as well as the secondary positron flux, can be parameterized as [49]:

$$\begin{aligned} \Phi_{\text{prim}, e^-}^{\text{bkg}} &= \frac{0.16\varepsilon^{-1.1}}{1 + 11\varepsilon^{0.9} + 3.2\varepsilon^{2.15}} \text{GeV}^{-1} \text{cm}^{-2} \text{s}^{-1} \text{sr}^{-1}, \\ \Phi_{\text{sec}, e^-}^{\text{bkg}} &= \frac{0.70\varepsilon^{0.7}}{1 + 11\varepsilon^{1.5} + 600\varepsilon^{2.9} + 580\varepsilon^{4.2}} \text{GeV}^{-1} \text{cm}^{-2} \text{s}^{-1} \text{sr}^{-1}, \\ \Phi_{\text{sec}, e^+}^{\text{bkg}} &= \frac{4.5\varepsilon^{0.7}}{1 + 650\varepsilon^{2.3} + 1500\varepsilon^{4.2}} \text{GeV}^{-1} \text{cm}^{-2} \text{s}^{-1} \text{sr}^{-1}, \end{aligned} \quad (29)$$

where $\varepsilon = E/(1 \text{ GeV})$ is a dimensionless parameter.

C. Results and Discussions

The net positron flux in the galactic medium is given by

$$(\Phi_{e^+})_{\text{Gal}} = (\Phi_{e^+})_{\text{bkg}} + \Phi_{e^+}(E, \vec{r}_\odot). \quad (30)$$

The second term in the above equation is given by Eq. (27), which depends on various factors: $b(E)$, $\lambda_D(E, E')$, $I(\lambda_D(E, E'))$, v_{e^+} , $(n_S)_\odot$ and the injection spectrum dN_{e^+}/dE' . The energy loss (due to inverse Compton scattering and synchrotron radiation with Galactic magnetic field) term $b(E)$ is determined by the photon density, and the strength of magnetic fields. Its value is taken to be $b(E) = 10^{-16}\varepsilon^2 \text{GeV s}^{-1}$ [49]. The number density of S DM in the Solar System is given by $(n_S)_\odot = \rho_\odot/M_S$, where $\rho_\odot \approx 0.3 \text{GeV/cm}^3$. In the energy range we are interested in, the value of v_{e^+} is taken approximately to be c , the velocity of light. The values of diffusion length $\lambda_D(E, E')$ and the corresponding halo function $I(\lambda_D(E, E'))$ are based on astrophysical assumptions [45, 46]. By considering different heights of the Galactic plane and different DM halo profiles the results may vary slightly. In the following,

the Galactic plane height is taken to be less than 4 kpc, which is referred to as the "MED" model [45, 46], and we have used the Navarro-Frenk-White (NFW) DM halo profile [50]

$$\rho(r) = \rho_{\odot} \left(\frac{r_{\odot}}{r} \right) \left(\frac{1 + \left(\frac{r_{\odot}}{r_s} \right)}{1 + \left(\frac{r}{r_s} \right)} \right)^2 \quad (31)$$

to determine the halo function $I(\lambda_D(E, E'))$, where $r_s \approx 20\text{kpc}$ and $r_{\odot} \approx 8.5\text{kpc}$.

We use the program DARKSUSY [51] to compute electron and positron fluxes from S annihilations $S^{\dagger}S \rightarrow h_2 h_2, h_2 \rightarrow \mu^+ \mu^-$. We then determine, for $100 \text{ GeV} \lesssim M_S \lesssim 1 \text{ TeV}$, what is the maximum annihilation cross section allowed for the fluxes not to exceed PAMELA observations. In this range, we found the approximate empirical upper bound:

$$\langle S_e \rangle \lesssim 1800 \times \left(\frac{M_S}{1 \text{ TeV}} \right)^{1.95}. \quad (32)$$

The constraint Eq. (32) only tells us that bigger boost factor are excluded. If one wants to fully account for the anomalous cosmic ray fluxes through DM annihilations, the boost factor gets lower-bounded, again in the $100 \text{ GeV} \lesssim M_S \lesssim 1 \text{ TeV}$ range:

$$\langle S_e \rangle \gtrsim 1000 \times \left(\frac{M_S}{1 \text{ TeV}} \right)^{1.85}. \quad (33)$$

If both Eqs. (32) and (33) are fulfilled, then cosmic ray fluxes are within 1 standard deviation of PAMELA data. Of course, if all PAMELA data have to be explained, $M_S \gtrsim 400 \text{ GeV}$ is required, given the annihilation channel $S^{\dagger}S \rightarrow h_2 h_2, h_2 \rightarrow \mu^+ \mu^-$.

Actually several constraints exist on large annihilation cross sections, relying on different physics, but all sensitive to DM annihilation products. When compared to the fiducial value of the annihilation cross section, these constraints apply in turn to the Sommerfeld enhancement $\langle S_e \rangle$. At high redshift, the energy deposition of the charged leptons may induce perturbations of the cosmic microwave background photon spectra [52], reionization and heating of the intergalactic medium [53], providing strong constraints. At the recombination time during which DM relative velocity is $\beta \sim 10^{-8}$, a bound on S_e is inferred [52]:

$$S_e \lesssim 480 \times \left(\frac{M_S}{1 \text{ TeV}} \right). \quad (34)$$

Stringent constraints arise from inverse Compton gamma rays in the Galaxy. The muons produced in DM annihilations subsequently decay into electrons. This population of electron yields irreducible high-energy gamma rays through inverse Compton on the Galactic radiation field. We consider the Fermi data released in [54], at galactic latitude $|b| > 10^\circ$ and the analysis of Ref. [55]. For a NFW profile and a final state into 4μ , the allowed boost factor is ~ 300 for a dark matter mass of 400 GeV . Notice that Ref. [56] considers a Galactic latitude closer to the Galactic center and is therefore more sensitive to the DM density profile. In this case and for a NFW profile the maximum allowed boost factor at $M_S = 400 \text{ GeV}$ is ~ 100 . The model is thus in great tension with the Pamela anomaly. However with an isothermal profile instead, a boost factor up to ~ 1000 is allowed, attenuating the constraints on the model parameter space. As for the extragalactic gamma ray constraints, discussed in Refs. [55, 57], they strongly depend on the assumptions on the history of structure formation. It turns out that the parameter space we are considering is allowed for a conservative choice of the halo concentration parameter, see Fig. 4 of [55] and Fig. 6 of Ref.[57] (which considers a two-muon final state case). For the cases we consider, constraints from recombination and from diffuse gamma rays are of the same order. In Figs.(3)-(5), we depicted the boost factor satisfying the constraints Eqs.(32-34) within a green (gray) band.

In Fig. (6), we show the comparison between the positron fraction obtained from S annihilations with the positron fraction observed by PAMELA, AMS and HEAT, for the two typical points defined in Table I at $M_S = 400 \text{ GeV}$. The quoted values of the couplings are inferred from Fig. (5), and provide a relic density in the WMAP7 range as well as saturate current direct detection bound. The first set of parameters is in a good agreement with the anomalous positron fraction observed by PAMELA. However, the corresponding boost factor $\langle S_e \rangle \sim 200$ is at the border line of gamma ray constraints coming from FermiLAT [55]-[57] and reionization [53]. The second set cannot entirely account for the excess measured by PAMELA since the largest boost factor allowed by direct detection is about 8. We conclude that in order to fully explain the positron fraction together with an observable cross section on nucleon, bigger values of $u \times f_{S\phi}$, and conversely lower values of the mixing angle are mandatory.

Point	$f_{S\phi}$	f_{HS}	u	θ_m	$\langle S_e \rangle$
1	0.82	10^{-2}	500	1.9×10^{-6}	195
2	0.1	10^{-2}	800	5×10^{-6}	8

TABLE I: Typical points used for the analysis of the PAMELA positron fraction. The DM mass is fixed at 400 GeV.

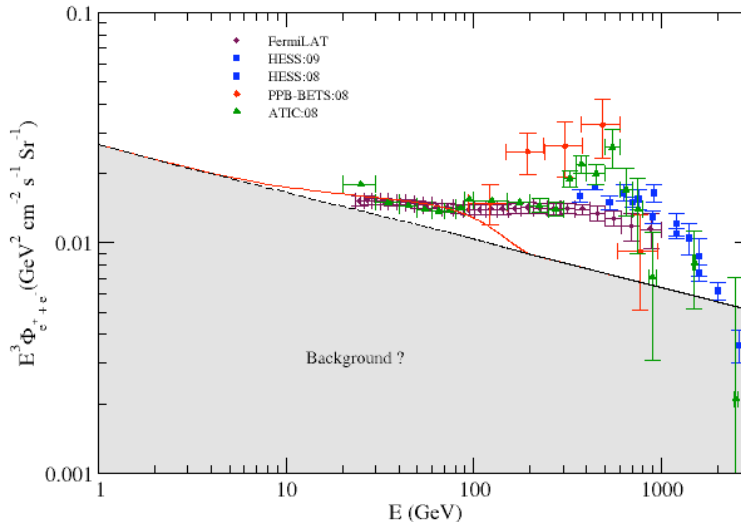


FIG. 7: Electron plus positron flux from $S^\dagger S \rightarrow 2\mu^+\mu^-$ at $M_S = 400$ GeV. The red solid line (black dashed line) stands for the illustrative point 1 (2) quoted in Table I.

Concerning the electron plus positron flux observed by FermiLAT, $M_S \sim 1$ TeV is necessary if the flux stems only from DM annihilations. However, for such high masses, the required boost factor is $\langle S_e \rangle \gtrsim 10^3$. Such a high value is in great tension with reionization constraints [53]. In Fig. (7), we compare FermiLAT, HESS, PPB-BETS and ATIC data on electron plus positron fluxes with the predictions of this model for the representative points mentioned in Table I, for which $M_S = 400$ GeV. The first point, depicted by a red solid line, yields $\langle S_e \rangle = 195$ and can fit PAMELA data as well as the low energy flux observed by FermiLAT. Of course, with $M_S = 400$ GeV, not all the energy range can be explained. The second point, depicted by a dashed black line and for which $\langle S_e \rangle = 8$, cannot account neither for the PAMELA results nor for the FermiLAT ones. In both cases, FermiLAT electron plus positron flux can only be explained by adding an extra source of astrophysical origin.

VI. CONCLUSIONS

In this paper we studied a hidden Abelian extension of the standard model. The DM is a complex scalar, singlet under the SM gauge group but charged under the hidden sector. We also introduce a light scalar Φ , whose non-zero vev u breaks $U(1)_H$ to a Z_2 symmetry under which all fields but S are even. As a result S is a stable DM candidate, with mass ranging from the GeV to the TeV scale. The three fields H , Φ and S couple together via three Higgs portal couplings. The physical scalars h and ϕ mix together with the mixing angle $\theta_m \propto f_{H\phi}$.

The relic density of S mainly results from the annihilation channel $S^\dagger S \rightarrow h_2 h_2$ through $f_{S\phi}$. All three portal couplings enter in the spin-independent DM-nucleon cross section. While the usual Higgs-mediated channel depends on f_{HS} , the mixing between h and ϕ provides an additional channel, mediated by the light scalar h_2 , which is $\propto u \times f_{S\phi} \times \theta_m$. Given the mass scales we consider, the main contribution to the direct detection signal actually comes from this mixing term. For the parameter space we scanned over, solutions are found saturating or exceeding current experimental bounds from XENON10 and CDMS-II, or are in the reach of sensitivity of XENON100. The model also provides indirect signatures of S through cosmic ray flux measurements. The main annihilation channel $S^\dagger S \rightarrow h_2 h_2$, followed by fast $h_2 \rightarrow \mu^+\mu^-$ decays, ends up in high-energy electron and positron fluxes. The suppression of S annihilations into standard Higgs compared to our dominant channel, together with the light mass of h_2 , entail

that no antiproton flux is expected at a significant level. A Sommerfeld enhancement of the current DM annihilation cross section occurs through the light h_2 exchange, which explains cosmic ray excess observations. This enhancement depends on $u \times f_{S\phi}$.

Interestingly, in this model, direct and indirect DM searches constrain same part of the parameter space. More precisely, in order to fully account for the anomalous positron fraction observed by PAMELA, large values of $u \times f_{S\phi}$ are required. Such large values give rise to large direct detection signals, saturating the current experimental exclusion limits. From this, an upper bound on the mixing angle is inferred. As an example, for $M_S = 400$ GeV and $u \times f_{S\phi} \sim 410$ GeV, θ_m should be less than 1.9×10^{-6} in order to satisfy simultaneously the current direct and indirect detection limits. We stress that in all models where the Sommerfeld enhancement occurs thanks to a light scalar that mixes with the Higgs particle, direct and indirect detection of dark matter are tightly connected.

Acknowledgments

N.S. would like to thank K. Kohri, J. McDonald and C. Balazs for useful discussions. This work is supported by the IISN and the Belgian Science Policy (IAP VI-11).

-
- [1] G. Jungman, M. Kamionkowski and K. Griest, Phys. Rept. **267**, 195 (1996) [arXiv:hep-ph/9506380];
G. Bertone, D. Hooper and J. Silk, Phys. Rept. **405**, 279 (2005) [arXiv:hep-ph/0404175].
- [2] Z. Ahmed *et al.* [The CDMS-II Collaboration], arXiv:0912.3592 [astro-ph.CO].
- [3] R. Bernabei *et al.*, Eur. Phys. J. C **67** (2010) 39 [arXiv:1002.1028 [astro-ph.GA]].
- [4] E. Armengaud *et al.*, Phys. Lett. B **687**, 294 (2010) [arXiv:0912.0805 [astro-ph.CO]].
- [5] V. N. Lebedenko *et al.*, Phys. Rev. D **80**, 052010 (2009) [arXiv:0812.1150 [astro-ph]].
- [6] J. Angle *et al.* [XENON collaboration], Phys. Rev. Lett. **100**, 021303 (2008), [arXiv:0706.0039 [astro-ph]].
- [7] G. Angloher *et al.*, arXiv:0809.1829 [astro-ph].
- [8] E. Aprile and L. Baudis [Xenon100 collaboration], Proc. Sci., IDM2008 (2008) 018, [arXiv:0902.4253 [astro-ph]].
- [9] O. Adriani *et al.* [PAMELA Collaboration], Nature **458**, 607 (2009) [arXiv:0810.4995 [astro-ph]].
- [10] M. Aguilar *et al.* [AMS-01 Collaboration], Phys. Lett. B **646**, 145 (2007) [arXiv:astro-ph/0703154].
- [11] S. W. Barwick *et al.* [HEAT Collaboration], Astrophys. J. **482**, L191 (1997) [arXiv:astro-ph/9703192];
J. J. Beatty *et al.*, Phys. Rev. Lett. **93** (2004) 241102 [arXiv:astro-ph/0412230].
- [12] F. Aharonian *et al.* [H.E.S.S. Collaboration], Phys. Rev. Lett. **97**, 221102 (2006) [Erratum-ibid. **97**, 249901 (2006)];
F. Aharonian *et al.* [H.E.S.S. Collaboration], Astron. Astrophys. **508** (2009) 561 [arXiv:0905.0105 [astro-ph.HE]].
- [13] A. A. Abdo *et al.* [The Fermi LAT Collaboration], Phys. Rev. Lett. **102**, 181101 (2009) [arXiv:0905.0025 [astro-ph.HE]].
- [14] J. Chang *et al.*, Nature **456**, 362 (2008).
- [15] S. Torii *et al.* [PPB-BETS Collaboration], arXiv:0809.0760 [astro-ph].
- [16] D. Hooper, P. Blasi and P. D. Serpico, JCAP **0901**, 025 (2009) [arXiv:0810.1527 [astro-ph]];
D. Hooper, A. Stebbins and K. M. Zurek, Phys. Rev. D **79**, 103513 (2009) [arXiv:0812.3202 [hep-ph]];
S. Profumo, arXiv:0812.4457 [astro-ph];
Y. Fujita, K. Kohri, R. Yamazaki, K. Ioka, Phys. Rev. D **80** (2009) 063003 [arXiv:0903.5298 [astro-ph.HE]];
M. Ahlers, P. Mertsch and S. Sarkar, Phys. Rev. D **80**, 123017 (2009) [arXiv:0909.4060 [astro-ph.HE]].
- [17] M. Aoki, S. Kanemura and O. Seto, Phys. Lett. B **685**, 313 (2010) [arXiv:0912.5536 [hep-ph]];
M. Farina, D. Pappadopulo and A. Strumia, Phys. Lett. B **688**, 329 (2010) [arXiv:0912.5038 [hep-ph]];
J. Hisano, K. Nakayama and M. Yamanaka, Phys. Lett. B **684**, 246 (2010) [arXiv:0912.4701 [hep-ph]];
M. Kadastik, K. Kannike, A. Racioppi and M. Raidal, arXiv:0912.3797 [hep-ph];
A. Bottino, F. Donato, N. Fornengo and S. Scopel, Phys. Rev. D **81**, 107302 (2010) [arXiv:0912.4025 [hep-ph]];
R. Allahverdi, B. Dutta and Y. Santoso, Phys. Lett. B **687**, 225 (2010) [arXiv:0912.4329 [hep-ph]];
A. Bandyopadhyay, S. Chakraborty, A. Ghosal and D. Majumdar, arXiv:1003.0809 [hep-ph].
- [18] V. Barger, W. Y. Keung, D. Marfatia and G. Shaughnessy, Phys. Lett. B **672**, 141 (2009) [arXiv:0809.0162 [hep-ph]];
M. Cirelli, M. Kadastik, M. Raidal and A. Strumia, Nucl. Phys. B **813**, 1 (2009) [arXiv:0809.2409 [hep-ph]];
J. Hisano, M. Kawasaki, K. Kohri and K. Nakayama, Phys. Rev. D **79**, 063514 (2009) [Erratum-ibid. D **80**, 029907 (2009)] [arXiv:0810.1892 [hep-ph]];
I. Cholis, D. P. Finkbeiner, L. Goodenough and N. Weiner, JCAP **0912**, 007 (2009) [arXiv:0810.5344 [astro-ph]];
E. Nezri, M. H. G. Tytgat and G. Vertongen, JCAP **0904**, 014 (2009) [arXiv:0901.2556 [hep-ph]];
L. Bergstrom, J. Edsjo and G. Zaharijas, Phys. Rev. Lett. **103**, 031103 (2009) [arXiv:0905.0333 [astro-ph.HE]];
P. Meade, M. Papucci, A. Strumia and T. Volansky, Nucl. Phys. B **831**, 178 (2010) [arXiv:0905.0480 [hep-ph]];
K. Kohri, J. McDonald and N. Sahu, Phys. Rev. D **81**, 023530 (2010) [arXiv:0905.1312 [hep-ph]].
- [19] C. Balazs, N. Sahu and A. Mazumdar, JCAP **0907**, 039 (2009) [arXiv:0905.4302 [hep-ph]];
E. Nardi, F. Sannino and A. Strumia, JCAP **0901**, 043 (2009) [arXiv:0811.4153 [hep-ph]];
S. Shirai, F. Takahashi and T. T. Yanagida, Phys. Lett. B **680**, 485 (2009) [arXiv:0905.0388 [hep-ph]];

- C. H. Chen, C. Q. Geng and D. V. Zhuridov, Eur. Phys. J. C **67**, 479 (2010) [arXiv:0905.0652 [hep-ph]];
- A. Arvanitaki, S. Dimopoulos, S. Dubovsky, P. W. Graham, R. Harnik and S. Rajendran, Phys. Rev. D **80**, 055011 (2009) [arXiv:0904.2789 [hep-ph]];
- A. Ibarra, D. Tran and C. Weniger, JCAP **1001**, 009 (2010) [arXiv:0906.1571 [hep-ph]];
- K. Kohri, A. Mazumdar, N. Sahu and P. Stephens, Phys. Rev. D **80**, 061302 (2009) [arXiv:0907.0622 [hep-ph]].
- [20] C. Arina, F. X. Josse-Michaux and N. Sahu, Phys. Lett. B **691**, 219 (2010) [arXiv:1004.0645 [hep-ph]].
- [21] D. P. Finkbeiner, T. R. Slatyer and N. Weiner, Phys. Rev. D **78** (2008) 116006 [arXiv:0810.0722];
S. M. Carroll, S. Mantry and M. J. Ramsey-Musolf, Phys. Rev. D **81** (2010) 063507, [arXiv: 0902.4461 [hep-ph]] ;
F. Chen, J. M. Cline and A. R. Frey, Phys. Rev. D **80**, 083516 (2009) [arXiv:0907.4746 [hep-ph]] ;
Q. H. Cao, I. Low and G. Shaughnessy, Phys. Lett. B **691**, 73 (2010) [arXiv:0912.4510 [hep-ph]].
- [22] V. Silveira and A. Zee, Phys. Lett. B **161** (1985) 136 ;
J. McDonald, Phys. Rev. D **50** (1994) 3637 [arXiv:hep-ph/0702143];
M. C. Bento, O. Bertolami, R. Rosenfeld and L. Teodoro, Phys. Rev. D **62** (2000) 041302 [arXiv:astro-ph/0003350];
C. P. Burgess, M. Pospelov and T. ter Veldhuis, Nucl. Phys. B **619** (2001) 709 [arXiv:hep-ph/0011335];
S. Andreas, T. Hambye and M. H. G. Tytgat, JCAP **0810** (2008) 034 [arXiv:0808.0255 [hep-ph]] ;
V. Barger, P. Langacker, M. McCaskey, M. Ramsey-Musolf and G. Shaughnessy, Phys. Rev. D **79** (2009) 015018 [arXiv:0811.0393 [hep-ph]].
- [23] B. Patt and F. Wilczek, arXiv:hep-ph/0605188.
- [24] E. Ma, Phys. Rev. D **73**, 077301 (2006) [arXiv:hep-ph/0601225] ;
R. Barbieri, L. J. Hall and V. S. Rychkov, Phys. Rev. D **74** (2006) 015007 [arXiv:hep-ph/0603188];
E. Ma, Mod. Phys. Lett. A **21** (2006) 1777 [arXiv:hep-ph/0605180];
L. Lopez Honorez, E. Nezri, J. F. Oliver and M. H. G. Tytgat, JCAP **0702**, 028 (2007) [arXiv:hep-ph/0612275];
N. Sahu and U. Sarkar, Phys. Rev. D **76**, 045014 (2007) [arXiv:hep-ph/0701062].
- [25] E. Komatsu *et al.*, arXiv:1001.4538 [astro-ph.CO].
- [26] R. Schabinger and J. D. Wells, Phys. Rev. D **72** (2005) 093007 [arXiv:hep-ph/0509209];
W. F. Chang, J. N. Ng and J. M. S. Wu, Phys. Rev. D **75** (2007) 115016 [arXiv:hep-ph/0701254];
D. Feldman, Z. Liu and P. Nath, Phys. Rev. D **75** (2007) 115001 [arXiv:hep-ph/0702123];
S. Gopalakrishna, S. Jung and J. D. Wells, Phys. Rev. D **78** (2008) 055002 [arXiv:0801.3456 [hep-ph]] ;
S. Gopalakrishna, S. J. Lee and J. D. Wells, Phys. Lett. B **680** (2009) 88 [arXiv:0904.2007 [hep-ph]] ;
K. Cheung, K. H. Tsao and T. C. Yuan, arXiv:1003.4611 [hep-ph].
- [27] D. Feldman, Z. Liu and P. Nath, Phys. Rev. D **79** (2009) 063509 [arXiv:0810.5762 [hep-ph]] ;
- [28] R. Barate *et al.* [LEP Working Group for Higgs boson searches collaboration], Phys. Lett. B **565** (2003), [arXiv:hep-ex/0306033].
- [29] CDF Collaboration and D0 Collaboration, arXiv:0903.4001 [hep-ex].
- [30] W. F. Chang, J. N. Ng and J. M. S. Wu, Phys. Rev. D **74**, 095005 (2006) [Erratum-ibid. D **79**, 039902 (2009)] [arXiv:hep-ph/0608068].
- [31] O. Adriani *et al.*, Phys. Rev. Lett. **102**, 051101 (2009) [arXiv:0810.4994 [astro-ph]].
- [32] M. Kawasaki, K. Kohri and T. Moroi, Phys. Rev. D **71** (2005) 083502 [arXiv:astro-ph/0408426];
K. Jedamzik and M. Pospelov, New J. Phys. **11** (2009) 105028 [arXiv:0906.2087 [hep-ph]].
- [33] D. Feldman, Z. Liu and P. Nath, Phys. Rev. Lett. **97**, 021801 (2006) [arXiv:hep-ph/0603039];
C. Amsler *et al.* (Particle Data Group), Phys. Lett. B **667**, 1 (2008).
- [34] D. O'Connell, M. J. Ramsey-Musolf and M. B. Wise, Phys. Rev. D **75** (2007) 037701 [arXiv:hep-ph/0611014].
- [35] S. Profumo, M. J. Ramsey-Musolf and G. Shaughnessy, JHEP **0708**, 010 (2007) [arXiv:0705.2425 [hep-ph]] ;
V. Barger, P. Langacker, M. McCaskey, M. J. Ramsey-Musolf and G. Shaughnessy, Phys. Rev. D **77**, 035005 (2008) [arXiv:0706.4311 [hep-ph]].
- [36] G. Belanger, F. Boudjema, A. Pukhov and A. Semenov, Comput. Phys. Commun. **180** (2009) 747 [arXiv:0803.2360 [hep-ph]].
- [37] N. D. Christensen and C. Duhr, Comput. Phys. Commun. **180** (2009) 1614 [arXiv:0806.4194 [hep-ph]].
- [38] J. Lavalley, Q. Yuan, D. Maurin and X. J. Bi, arXiv:0709.3634 [astro-ph].
- [39] M. Ibe, H. Murayama and T. T. Yanagida, Phys. Rev. D **79** (2009) 095009 [arXiv:0812.0072 [hep-ph]].
- [40] J. Hisano, S. Matsumoto, M. Nagai, O. Saito and M. Senami, Phys. Lett. B **646** (2007) 34 [arXiv:hep-ph/0610249];
M. Cirelli, A. Strumia and M. Tamburini, Nucl. Phys. B **787** (2007) 152 [arXiv:0706.4071 [hep-ph]].
J. March-Russell, S. M. West, D. Cumberbatch and D. Hooper, JHEP **0807**, 058 (2008) [arXiv:0801.3440 [hep-ph]] ;
N. Arkani-Hamed, D. P. Finkbeiner, T. R. Slatyer and N. Weiner, Phys. Rev. D **79**, 015014 (2009) [arXiv:0810.0713 [hep-ph]].
- [41] J. Kopp, T. Schwetz and J. Zupan, JCAP **1002**, 014 (2010) [arXiv:0912.4264 [hep-ph]].
- [42] S. Yellin, Phys. Rev. D **66**, 032005 (2002) [arXiv:physics/0203002].
- [43] J. Angle *et al.* [XENON10 collaboration], Phys. Rev. D **80**, 115005 (2009) [arXiv:0910.3698 [astro-ph]].
- [44] R. Koch, Z.Physik C **15** 161 (1982) ;
J. Gasser, H. Leutwyler and M. E. Sainio, Phys. Lett. B **253** 260 (1991) ;
M. M. Pavan, R. A. Arndt, I. I. Strakovski and R. L. Workman, PiN Newslett. **16** 110 (2002) ;
A. Bottino, F. Donato, N. Fornengo and S. Scopel, Phys. Rev. D **78** 083520 (2008), [arXiv:0806.4099].
- [45] T. Delahaye, R. Lineros, F. Donato, N. Fornengo and P. Salati, Phys. Rev. D **77** (2008) 063527 [arXiv:0712.2312 [astro-ph]].
- [46] M. Cirelli, R. Franceschini and A. Strumia, Nucl. Phys. B **800**, 204 (2008) [arXiv:0802.3378 [hep-ph]].

- [47] J. Hisano, S. Matsumoto, O. Saito and M. Senami, Phys. Rev. D **73**, 055004 (2006) [arXiv:hep-ph/0511118].
- [48] I. V. Moskalenko and A. W. Strong, Astrophys. J. **493**, 694 (1998) [arXiv:astro-ph/9710124].
- [49] E. A. Baltz and J. Edsjo, Phys. Rev. D **59**, 023511 (1999) [arXiv:astro-ph/9808243].
- [50] J.F. Navarro, C.S. Frenk and S.D.M. White, Astrophys.J.**462**, 563 (1996).
- [51] P. Gondolo, J. Edsjo, P. Ullio, L. Bergstrom, M. Schelke and E. A. Baltz, JCAP **0407**, 008 (2004) [arXiv:astro-ph/0406204];
- [52] S. Galli, F. Iocco, G. Bertone and A. Melchiorri, Phys. Rev. D **80** (2009) 023505 [arXiv:0905.0003 [astro-ph.CO]];
T. R. Slatyer, N. Padmanabhan and D. P. Finkbeiner, Phys. Rev. D **80** (2009) 043526 [arXiv:0906.1197 [astro-ph.CO]].
- [53] G. Huetsi, A. Hektor and M. Raidal, Astron. Astrophys. **505** (2009) 999 [arXiv:0906.4550 [astro-ph.CO]];
M. Cirelli, F. Iocco and P. Panci, JCAP **0910** (2009) 009 [arXiv:0907.0719 [astro-ph.CO]].
- [54] A. A. Abdo *et al.* [The Fermi-LAT collaboration], Phys. Rev. Lett. **104** (2010) 101101 [arXiv:1002.3603 [astro-ph.HE]].
- [55] G. Huetsi, A. Hektor and M. Raidal, JCAP **1007**, 008 (2010) [arXiv:1004.2036 [astro-ph.HE]].
- [56] M. Papucci and A. Strumia, JCAP **1003**, 014 (2010) [arXiv:0912.0742 [hep-ph]].
- [57] A. A. Abdo *et al.* [Fermi-LAT Collaboration], JCAP **1004**, 014 (2010) [arXiv:1002.4415 [astro-ph.CO]].